A novel thermally biased mechanical energy conversion cycle

Ian M. McKinley, Sam Goljahi, Christopher S. Lynch, and Laurent Pilon[a)]
Mechanical and Aerospace Engineering Department, Henry Samueli School of Engineering and Applied Science, University of California, Los Angeles, Los Angeles, California 90095, USA

This paper demonstrates a new power cycle for direct conversion of mechanical energy into electrical energy under a thermal bias. The cycle consisted sequentially of (i) an electric poling process under zero stress, (ii) an isoelectric process consisting of applying a uniaxial compressive stress σ_H followed by (iii) an electric de-poling process under constant compressive stress, and finally (iv) an isoelectric process consisting of removing the compressive stress. The new cycle was performed at constant bias-temperature T_b. It was demonstrated on [001]-poled $0.72PbMg_{1/3}Nb_{2/3}O_3$-$0.28PbTiO_3$ single crystals. The power density increased with increasing cycle frequency and compressive stress for frequency up to 1 Hz. Maximum energy and power densities of 44 J/l/cycle and 44 W/l were achieved at 1 Hz for bias-temperature T_b of $80\,°C$ and electric field cycled between 0.2 and 0.8 MV/m with compressive stress $\sigma_H = 25.13$ MPa. This was attributed to a tetragonal-monoclinic-orthorhombic phase transition sequence. The material efficiency reached up to 87% and exceeded that of a similar thermomechanical power cycle performed on pyroelectric material. Finally, a physical model predicting the power density was derived and yielded accurate predictions of experimental data for all bias-temperatures considered and cycle frequency up to 1 Hz. © *2013 AIP Publishing LLC.* [http://dx.doi.org/10.1063/1.4846735]

I. INTRODUCTION

Rising awareness in sustainable and efficient energy technologies has stimulated efforts in scavenging thermal and mechanical energies. In 2012, an estimated 60% of the energy consumed in the United States was rejected mainly in the form of low grade waste heat.[1] Methods for harvesting low grade waste heat include Stirling engines,[2] organic Rankine cycles,[3] and thermoelectric devices.[4,5] Stirling engines and organic Rankine cycles convert thermal energy into mechanical energy. Thermoelectric devices make use of the Seebeck effect to convert a steady-state temperature difference at the junction of two dissimilar metals or semiconductors directly into electrical energy.[4] Waste mechanical energy in the form vibrations, shocks, or strains can also be harvested.[6] Methods for direct mechanical to electrical energy conversion include electromagnet, electrostatic, and electroactive polymers generators.[6] Electromagnetic generators rely on time-varying magnetic field caused by the relative motion between a magnet and a coil to generate electrical energy.[6] Electrostatic generators rely on temporal variations in the capacitance of a structure caused by mechanical motion to generate electrical energy.[6] By contrast, electroactive polymers generate electrical energy in response to a change in shape due to mechanical deformations.[6] Alternatively, ferroelectric materials have the ability to convert both thermal and mechanical energy directly into electricity. They possess a temperature and stress-dependent

polarization and constitute a subclass of pyroelectric materials themselves a subclass of piezoelectric materials.[7]

This study presents a novel cycle performed on ferroelectric materials that converts time-dependent compressive stress oscillations under constant bias-temperature directly into electricity. This new cycle was demonstrated on commercially available [001]-poled lead magnesium niobate-lead titanate $0.72PbMg_{1/3}Nb_{2/3}O_3$-$0.28PbTiO_3$ (PMN-28PT) single crystals.

II. BACKGROUND

A. Dielectric hysteresis loops

Figure 1(a) presents the isothermal bipolar hysteresis curves (*D-E* loops) in the electric displacement *D* versus electric field *E* diagram for a typical ferroelectric material at constant temperature T_b under compressive stress σ equal to 0 and σ_H. The *D-E* loops under any compressive stress traveled in the counter-clockwise direction. The electric displacement *D* of a ferroelectric material at temperature *T* under electric field *E* and compressive stress σ can be expressed as[7,8]

$$D(E, T, \sigma) = \varepsilon_0 \varepsilon_r(T, \sigma)E + P_s(T, \sigma), \quad (1)$$

where ε_o is the vacuum permittivity equal to 8.854×10^{-12} F/m and $\varepsilon_r(T, \sigma)$ is the large-field dielectric constant of the material at temperature *T* and under stress σ. The saturation polarization $P_s(T, \sigma)$ is equal to the electric displacement in the linear fit of *D* versus *E* at large-field extrapolated to zero electric field[9] and the slope of this linear fit corresponds to the product $\varepsilon_0 \varepsilon_r(T, \sigma)$.

[a)]Author to whom correspondence should be addressed. Electronic mail: pilon@seas.ucla.edu. Tel.: +1 (310)-206-5598. Fax: +1 (310)-206-4830.
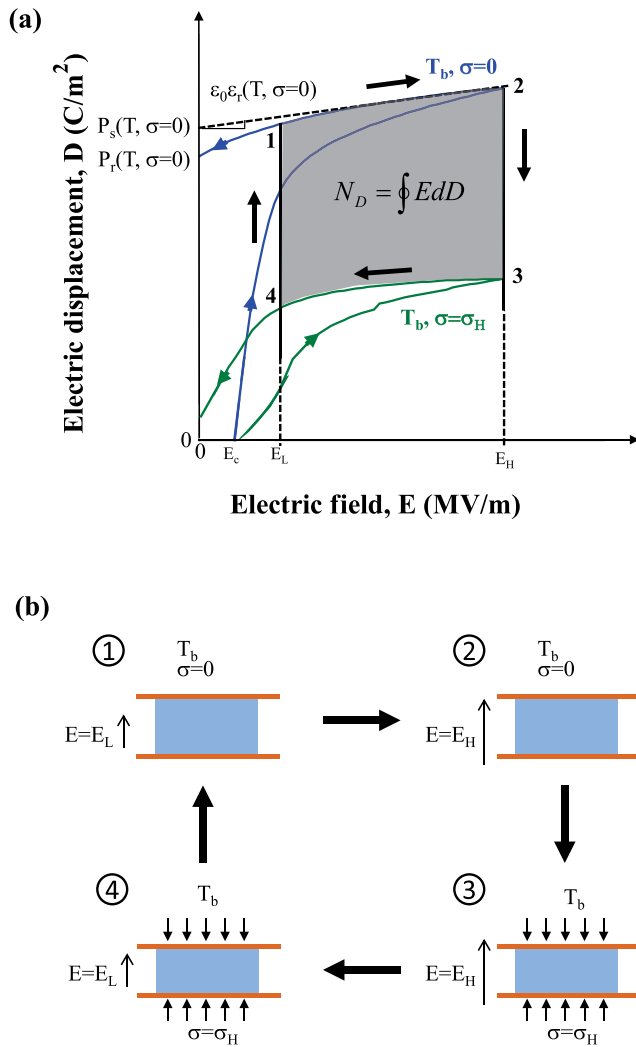
(a)

(b)

FIG. 1. (a) Two-dimensional projection of the new power cycle in the *D-E* plane. Electric displacement versus electric field loops for uniaxial stress $\sigma = 0$ and for σ_H at temperature T_b. The electrical energy generated per cycle is represented by the grey area enclosed between 1–2–3–4. (b) The thermal, electrical, and stress states of the ferroelectric sample during each point of the new power cycle.

B. Single crystal PMN-*x*PT

Single crystal PMN-*x*PT possesses large piezoelectric constants near the morphotropic phase boundary (MPB) separating the rhombohedral and tetragonal phases.[10] This MPB corresponds to *x* ranging between 27.5 and 33 mol. %.[11] Zhou *et al.*[12] compared the performance of PMN-*x*PT with *x* equal to 28, 30, and 32 mol. % and determined that PMN-28PT was the preferred composition for transducer, sensor, and actuator applications due to its advantageous piezoelectric properties in a broad temperature range. The electric field versus temperature (E-T) phase diagram of $\langle 001 \rangle$ PMN-28PT under zero stress indicates that the material has a monoclinic-tetragonal (M-T) phase boundary around 90 °C under zero electric field.[13] This phase boundary temperature decreases to 85 °C and 70 °C as the electric field increases from 0 to 0.2 and 0.8 MV/m, respectively.[13] At room temperature under zero electric field, the material is in the rhombohedral phase[14] and undergoes a rhombohedral-monoclinic (R-M) phase transition at 0.2 MV/m.[13] In addition, for [001] PMN-32PT, the electric field corresponding to the *R-M* and *M-T* phases boundaries increases with increasing uniaxial compressive stress for a given temperature.[15] McLaughlin *et al.*[15] found that a depolarized orthorhombic (O) phase occurs in [001] PMN-32PT under large uniaxial stress and small electric field. In addition, the authors found that rhombohedral to orthorhombic (R-O) phase transition occurred with the application of compressive stress at temperatures less than 60 °C.[15] However, at temperatures greater than 60 °C, a direct monoclinic M_A to orthorhombic (M_A-O) phase transition occurred upon application of a compressive stress.[15] Furthermore, the O-M_A and M_A-T phase transitions occurring at high temperature exhibit small hysteresis characteristic of continuous polarization rotation.[15] This suggests that there are continuous rather than abrupt phase transitions and multiple phases may coexist.[15,16] Finally, the phase boundaries in PMN-*x*PT are frequency-dependent typical of relaxor behavior.[17] For example, Chen *et al.*[17] found the peak of the dielectric constant as a function of temperature for PMN-20PT ceramics heated at 1 K/min to vary from 84 to 96 °C for frequency ranging from 0.1 to 100 kHz.

C. Previous power cycles on ferroelectric materials

The Olsen cycle performed on pyroelectric materials can convert temporal temperature oscillations directly into electricity.[18] This cycle consists of two isothermal and two iso-electric field processes in the *D-E* diagram and is analogous to the Ericsson cycle, in which a working fluid undergoes two isothermal and two isobaric processes in the pressure-volume diagram.[18] In addition, time-dependent mechanical deformations imposed on piezoelectric materials connected to an external electrical load can generate electricity.[19,20] These mechanical deformations can be small deflections at high frequency due to vibrations[19] or can be large strains due to the application of large cyclic compressive stress.[20] Furthermore, the thermomechanical power cycle demonstrated by McKinley *et al.*[21] performed on ferroelectric materials utilizes time-dependent temperature and compressive stress oscillations to convert both thermal and mechanical energies directly into electricity. The first process consists of an isothermal increase in electric field from E_L to E_H at T_{cold}, performed in the absence of compressive stress. The second process corresponds to simultaneously compressing the sample under compressive stress σ_H and heating it up to T_{hot}. The third process consists of an isothermal decrease in electric field from E_H to E_L at T_{hot} under compressive stress σ_H. Finally, the fourth process closes the cycle by simultaneously cooling the sample to T_{cold} and removing the loading under constant electric field E_L. This cycle was demonstrated on 3 mm thick $\langle 001 \rangle$-oriented PMN-28PT single crystals and achieved larger energy and power densities than the Olsen cycle for lower operating temperatures.[21] This was realized (i) by combining both piezoelectric and pyroelectric energy conversion and (ii) by increasing the cycle frequency by quickly forcing the material into a specific state using mechanical stress instead of heating and cooling which are inherently slow. However, the heat input still dominated the energy consumption of the thermomechanical power cycle at low cycle frequencies and negatively affected the material efficiency.[21]

D. Material efficiency

The material efficiency of a power cycle is typically defined as the ratio of the energy produced by the material to the energy consumed by performing the cycle. Overall, the material efficiency of the thermomechanical cycle can be expressed as

$$\eta = \frac{N_D}{Q_{in} + W_{in}}, \tag{2}$$

where N_D is the electrical energy produced per unit volume of the material per cycle while Q_{in} and W_{in} are the thermal energy and mechanical work provided per unit volume of the material during the cycle. The area enclosed by the cycle in the D-E diagram corresponds to the generated energy density N_D. It is expressed in J/l/cycle $(1\,\text{J/l/cycle} = 1\,\text{kJ/m}^3/\text{cycle})$ and defined as[18]

$$N_D = \oint E dD. \tag{3}$$

The power density P_D is the amount of energy generated per unit time per unit volume of pyroelectric material. It is expressed in W/l $(1\,\text{W/l} = 1\,\text{kJ/m}^3)$ and defined as $P_D = N_D f$ where f is the cycle frequency. The overall cycle frequency (in Hz) is defined as $f = (\tau_{12} + \tau_{23} + \tau_{34} + \tau_{41})^{-1}$ with τ_{ij} corresponding to the duration of process i-j.

The thermal energy consumed per unit volume of material during the cycle may be expressed as

$$Q_{in} = \oint \rho c_p(T) dT, \tag{4}$$

where $c_p(T)$ and ρ are the specific heat and density of the ferroelectric material expressed in J/kg K and kg/m^3, respectively. In addition, the mechanical work W_{in} per unit volume of material can be expressed as

$$W_{in} = \oint \sigma(x) dx, \tag{5}$$

where x represents the strain in the longitudinal direction parallel to the polarization. For ferroelectric materials undergoing phase transitions, the relationship between σ and x is typically non-linear[22,23] and should be estimated from stress-strain curves.[24]

Here, we present a new cycle using variable uniaxial compressive stress in addition to electric field cycling but at a fixed temperature. We hope that this new cycle can achieve larger cycle efficiency than the thermomechanical cycle by reducing the required heat input. Single crystal PMN-28PT was used for its advantageous piezoelectric properties and for comparison purposes.

III. THERMALLY BIASED MECHANICAL POWER CYCLE

A. Principle

Figure 1(a) illustrates the new power cycle in the D-E diagram overlaid with the corresponding isothermal bipolar D-E loops at constant bias-temperature T_b under zero stress

and under compressive stress σ_H. Figure 1(b) schematically illustrates the practical implementation of the new power cycle and the stress, temperature, and electric field imposed in each state. Process 1–2 consists of an isothermal increase in electric field from E_L to E_H, performed in the absence of compressive stress. Process 2–3 corresponds to compressing the sample under stress σ_H. Process 3–4 consists of an isothermal decrease in electric field from E_H to E_L under compressive stress σ_H. Finally, process 4-1 closes the cycle by removing the loading under constant electric field E_L. The area enclosed by the four processes in the D-E diagram, shown in Figure 1(a), corresponds to the generated energy density N_D defined by Eq. (3). It is evident that the energy density N_D can be increased by increasing the electric field span E_H-E_L and/or increasing the change in electric displacement during processes 2–3 and 4-1.

B. Experiments

1. Samples

PMN-28PT was chosen to demonstrate the thermomechanical power cycle[21] for its strong piezoelectric response in a broad temperature range.[12] Single crystal samples of PMN-28PT were purchased from Sinoceramics, LLC. The samples were $5 \times 5 \times 3$ mm^3 and poled in the [001]-direction. The two 5×5 mm^2 faces of each sample were entirely coated with Cr/Au electrodes. Two strain gages were mounted to opposite 5×3 mm^2 faces of one of the samples to measure longitudinal strain (parallel to the polarization direction).

2. Experimental setup

The experimental setup included an electrical and a thermomechanical subsystem. The electrical subsystem was a Sawyer-Tower circuit identical to that used in our previous studies that simultaneously measured electric field and electric displacement.[25–30] Figure 2 shows a schematic of the thermomechanical subsystem used to perform the novel power cycle. The subsystem consisted of a spring return air cylinder (McMaster-Carr 6498K252) vertically actuated using compressed air at a maximum pressure of 469 kPa. A 24 V DC solenoid valve was used to control the extension and contraction of the cylinder rod applying pressure on the sample between two copper rods. The PMN-28PT sample was sandwiched between two copper tapes used to provide electrical contact between the sample's electrodes and the wires. A 0.14 mm thick Kapton film was used to electrically isolate the sample's electrodes from the copper rods. The sample was placed inside an acrylic support structure submerged in a heated silicone oil bath. A 100-Watt cartridge heater was imbedded in a 1.27 cm thick aluminum plate serving as a heat source to the oil bath. A type-K thermocouple was embedded at the center of this heating block whose temperature was maintained at T_H with an Omega CN-7823 proportional integral derivative (PID) temperature controller. The corresponding sample bias-temperature T_b was measured by a type-K thermocouple placed on the sample. After the desired steady-state temperature was reached, this second
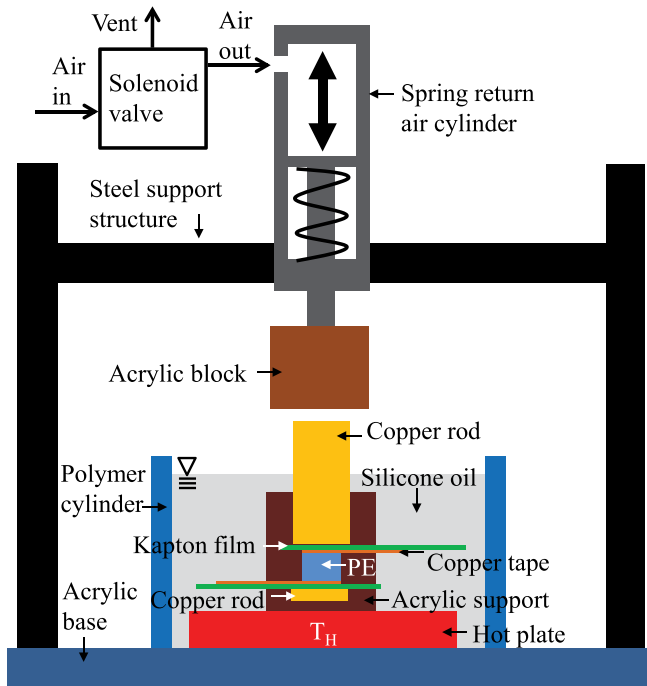
FIG. 2. Schematic of the thermomechanical subsystem used to create the temperature bias and to apply compressive stress during the new thermally biased mechanical power cycle depicted in Figure 1. Dimensions are not to scale.

thermocouple was removed prior to performing the cycle so that it did not electrically interfere with electrical measurements performed on the sample.

In addition, a servo-hydraulic test frame described in Ref. 22 was used in place of the spring return air cylinder for mechanical characterization of the sample during the cycle. The compressive force applied by this servo-hydraulic mechanism was computer-controlled enabling strain to be measured as a function of stress while also simultaneously measuring electric field and electric displacement.

3. Experimental procedure

First, isothermal bipolar D-E hysteresis loops of [001] PMN-28PT were collected for bias-temperature of 22, 80, and 100 °C and compressive stress varying from 0 to 25.13 MPa. The dielectric properties of PMN-28PT were estimated from the isothermal bipolar D-E loops. The saturation polarization $P_s(T, \sigma)$ and the large-field dielectric constant $\varepsilon_r(T, \sigma)$ were evaluated by linearly fitting the bipolar D-E loops corresponding to a decrease in electric field from 0.75 to 0.5 MV/m according to Eq. (1) and as illustrated in Figure 1(a).

Second, the new cycle was performed so that the duration of each process was equal, i.e., $\tau_{12} = \tau_{23} = \tau_{34} = \tau_{41}$. The new power cycle was executed for frequency ranging from 0.5 to 3 Hz by varying τ_{ij} between 1 and 0.083 s, respectively. The sample bias-temperature T_b varied from 22 to 100 °C, and the uniaxial stress σ_H applied during processes 2–3 and 3–4 ranged from 0 to 35.67 MPa. The low and high electric fields E_L and E_H were fixed at 0.2 and 0.8 MV/m, respectively.

In addition, the new power cycle was performed at very low cycle frequency ($f \sim 0.004$ Hz) in the servo-hydraulic test frame[22] while the electric field, electric displacement, stress, and strain were simultaneously measured. The load frame measured the applied force ranging from 0 to 850 N corresponding to stress of 0 to 34 MPa. The energy density generated per cycle N_D was evaluated by numerically integrating experimental data for D versus E according to Eq. (3) using the trapezoidal rule. The mechanical work done per cycle W_{in} was evaluated by numerically integrating experimental data for σ versus x according to Eq. (5) using the trapezoidal rule. Finally, the material efficiency η given by Eq. (2) was estimated.

C. Physical modeling

Recently, Kandilian *et al.*[25] developed a model to predict the energy density generated by the Olsen cycle. This model can easily be adapted to predict the power density generated by materials undergoing the present thermally biased mechanical cycle. According to Eq. (1), the large-field dielectric constant $\varepsilon_r(T, \sigma)$ and the saturation polarization $P_s(T, \sigma)$ are functions of both temperature and compressive stress. Assuming the D-E path of the new cycle follows that of the D-E loops at bias-temperature T_b both under zero and σ_H stress, the power density of the new cycle at frequency f can be expressed as

$$P_D = f(E_H - E_L)\left\{ \frac{\varepsilon_0}{2}[\varepsilon_r(T_b, 0) - \varepsilon_r(T_b, \sigma_H)](E_H + E_L) \right.$$
$$\left. + P_s(T_b, 0) - P_s(T_b, \sigma_H) \right\}. \tag{6}$$

This model could enable the rapid determination of the power density of materials undergoing the new cycle from intrinsic dielectric properties of PMN-28PT without physically having to perform the cycle. But first, it must be validated experimentally.

IV. RESULTS AND DISCUSSION

A. Isothermal bipolar *D-E* loops

Figure 3 plots isothermal bipolar D-E loops measured at 0.1 Hz on [001] PMN-28PT samples for bias-temperature T_b of (a) 80 °C and (b) 100 °C under mechanical loading ranging between 0 and 25.13 MPa. The D-E loops were closed and consecutive D-E loops overlapped for any temperature and compressive stress considered. This indicates that leakage current through the sample was negligibly small. Figure 3 illustrates that the D-E loops gradually became slimmer with increasing compressive stress. This behavior is indicative of continuous polarization rotation and was previously observed with [001] PMN-32PT.[16] Figure 4 shows (a) the saturation polarization $P_s(T, \sigma)$ and (b) the large-field dielectric constant $\varepsilon_r(T, \sigma)$ retrieved from the isothermal bipolar D-E loops for temperatures 22, 80, and 100 °C and compressive stress between 0 and 25.13 MPa. Each data point represents the average over three D–E loops. The error bars have been omitted because they
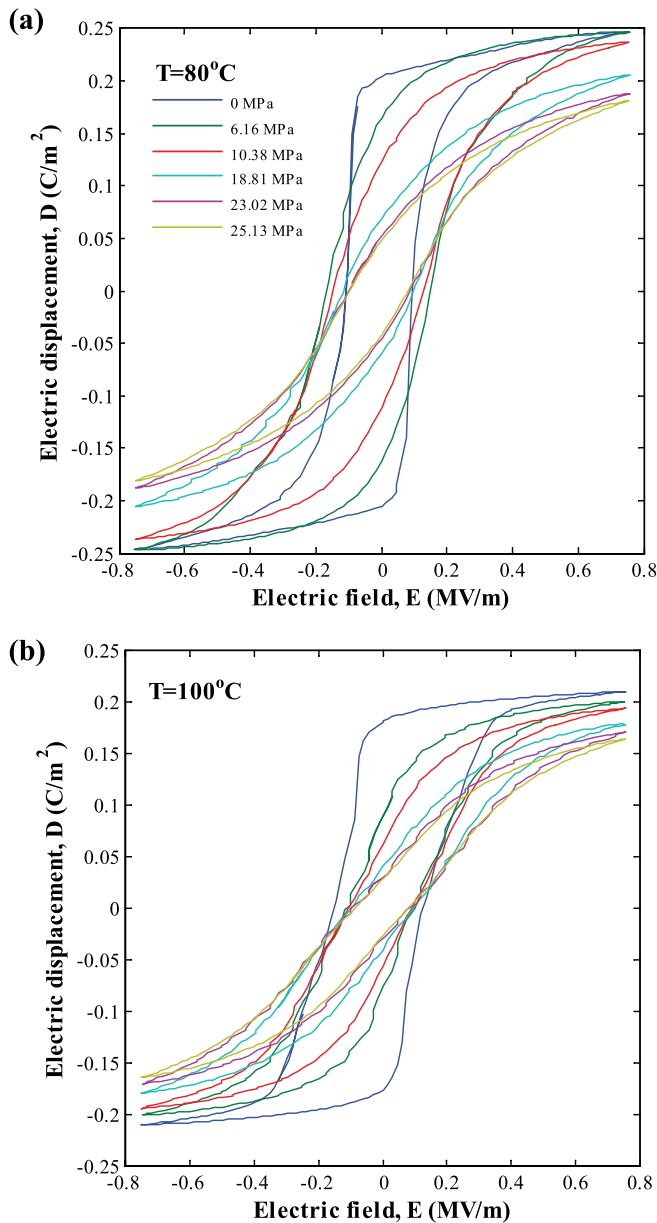
FIG. 3. Isothermal bipolar *D-E* loops of [001] PMN-28PT at 0.1 Hz for temperatures (a) 80 °C and (b) 100 °C and compressive stress σ between 0 and 25.13 MPa.
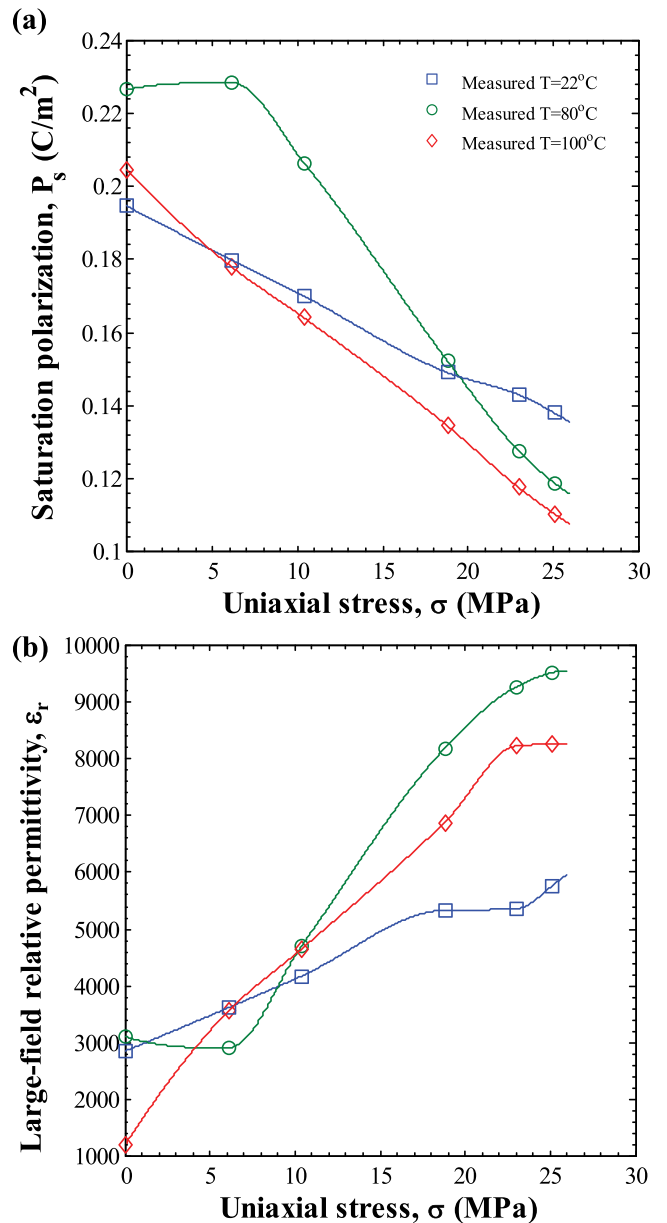

FIG. 4. (a) Saturation polarization $P_s(T, \sigma)$ and (b) large-field relative permittivity $\varepsilon_r(T, \sigma)$ as a function of uniaxial stress retrieved from the isothermal bipolar *D-E* loops of PMN-28PT at 0.1 Hz for temperatures 22, 80, and 100 °C (Figure 3). The solid lines correspond to the piecewise cubic hermite interpolating polynomial fit.

fell within the data markers. In addition, Figure 4 also shows the piecewise cubic hermite interpolating polynomial fit of the properties for each temperature considered. Figure 4(a) indicates that the saturation polarization P_s decreased nearly linearly with increasing stress at 22 and 100 °C. This behavior is also characteristic of continuous polarization rotation corresponding to continuous phase transitions.[15,16] On the other hand, at 80 °C, the saturation polarization was nearly constant below 6.16 MPa and decreased linearly with compressive stress beyond. This can be attributed to phase transition from tetragonal to monoclinic at 80 °C and compressive stress between 6.16 and 10.38 MPa. Indeed, at 80 °C, [001] PMN-28PT assumes the tetragonal phase under zero stress and electric field above 0.4 MV/m.[13] In addition, [001] PMN-32PT was reported to assume the monoclinic phase at 80 °C under stress above 10 MPa and electric field below

1 MV/m.[15] As stress increased from 0 to 25 MPa, the largest change in saturation polarization occurred at 80 °C, while the smallest change occurred at 22 °C. Figure 4(b) indicates that the large-field relative permittivity increased with increasing compressive stress for all temperatures considered. This behavior is consistent with bipolar *D-E* loops reported for [001] PMN-30PT (Ref. 23) and [001] PMN-32PT (Ref. 16) at room temperature for compressive stress up to 30 MPa.

B. Thermally biased mechanical power cycle

1. Demonstration

Figure 5 depicts, in the *D–E* diagram, the new mechanical power cycle performed at 1 Hz at bias-temperature
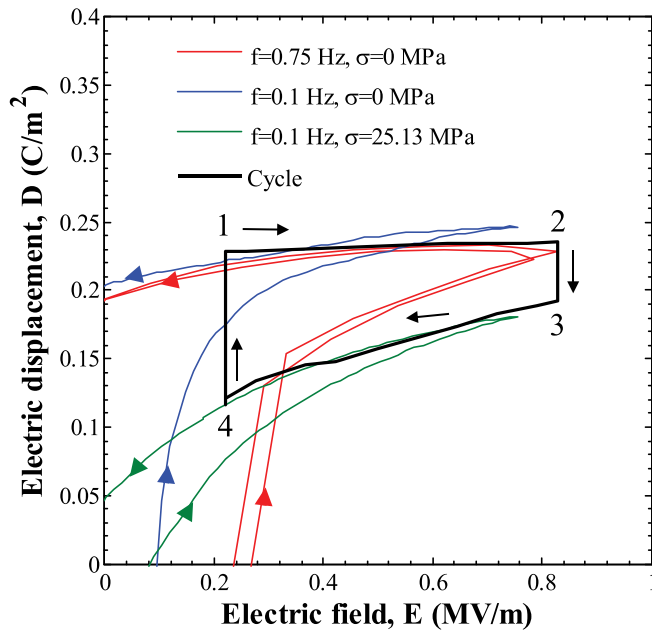
FIG. 5. Isothermal bipolar *D-E* loops collected at 0.1 or 0.75 Hz and experimental power cycle performed at frequency $f = 1$ Hz on PMN-28PT for electric field between $E_L = 0.2$ MV/m and $E_H = 0.8$ MV/m at $T_b = 80\,°C$ and compressive stress between $\sigma = 0$ and $\sigma_H = 25.13$ MPa. The power cycle was vertically displaced to match the *D-E* loop at $T = 80\,°C$ and $\sigma_H = 25.13$ MPa.

$T_b = 80\,°C$. The electric field was cycled between $E_L = 0.2$ MV/m and $E_H = 0.8$ MV/m. A compressive stress of $\sigma_H = 25.13$ MPa was applied during processes 2–3 and 3–4. The cycle traveled in the clockwise direction and therefore produced electrical energy. Figure 5 also shows the isothermal bipolar *D-E* loops measured at $80\,°C$ at 0.1 Hz under zero stress and $\sigma_H = 25.13$ MPa as well as at 0.75 Hz under zero stress. Note that the rate of electric field change dE/dt for the *D-E* loops at 0.1 Hz and 0.75 Hz was 0.3 and 2.4 MV/m s, respectively. Processes 1–2 and 3–4 of the cycle performed at 1 Hz corresponded to a time rate of change in electric field of 2.4 MV/m s. However, Figure 5 indicates that at the frequencies considered, the *D-E* loops were independent of dE/dt. In addition, the power cycle shown was vertically translated to match the electric displacement of the *D-E* loop for T_b and $\sigma = 25.13$ MPa, as performed by Kandilian *et al.*[25] It is evident that the cycle closely followed the bipolar *D-E* loops corresponding to the conditions of the cycle. Thus, using the properties $P_s(T, \sigma)$ and $\varepsilon_r(T, \sigma)$ previously retrieved from the bipolar *D-E* loops at 0.1 Hz was appropriate to predict the power density based on Eq. (6).

Given the phase diagram of PMN-28PT reported in Ref. 13 at frequency of 10 Hz, we speculate that, at bias-temperature of $80\,°C$, PMN-28PT was in the tetragonal *T* phase at both state 1 and 2 of the cycle. This is supported by the fact that (i) the coercive electric field in the *D-E* loops at low frequency of 0.1 Hz was around 0.1 MV/m and (ii) the change in electric displacement between these states was small as illustrated in Figure 5. In addition, we speculate that the application of compressive stress during process 2–3 caused the sample to undergo a phase transition into the monoclinic M_A phase, as suggested by the *T*-M_A phase

transition occurring in [001] PMN-32PT at 0.8 MV/m and $80\,°C$ under $\sigma = 13$ MPa.[15] Furthermore, the decrease in electric field during process 3–4 caused another phase transition into the depolarized orthorhombic *O* phase. This was suggested by the M_A-*O* phase transition in [001] PMN-32PT occurring at 0.2 MV/m and $80\,°C$ under $\sigma = 20$ MPa.[15] Finally, during process 4-1, when stress was removed at constant electric field 0.2 MV/m, the sample transitioned back to the tetragonal phase. Thus, during the cycle at $80\,°C$, the sample successfully alternated between a depolarized state and a highly polarized state corresponding to a large change in electric displacement and a large energy density.

2. Effect of temperature and compressive stress

Figure 6 shows the power density generated by the new power cycle as a function of applied compressive stress σ_H for bias-temperature T_b ranging between 22 and $100\,°C$. Here, the frequency was fixed at 1 Hz while the electric field was cycled between 0.2 and 0.8 MV/m. Each data point represents an average of five cycles and the error bars correspond to one standard deviation or 63% confidence interval. Figure 6 indicates that the power density increased nearly linearly with increasing σ_H for any given bias-temperature T_b. For T_b above $80\,°C$, the power density decreased and was nearly identical for 90 and $100\,°C$. In fact, the largest power density of 44 W/l was achieved for bias-temperature of $80\,°C$ with a compressive stress of 25.13 MPa. This optimum performance can be explained by the tetragonal to monoclinic to orthorhombic phase transition sequence previously discussed. On the other hand, for bias-temperatures of 90 and
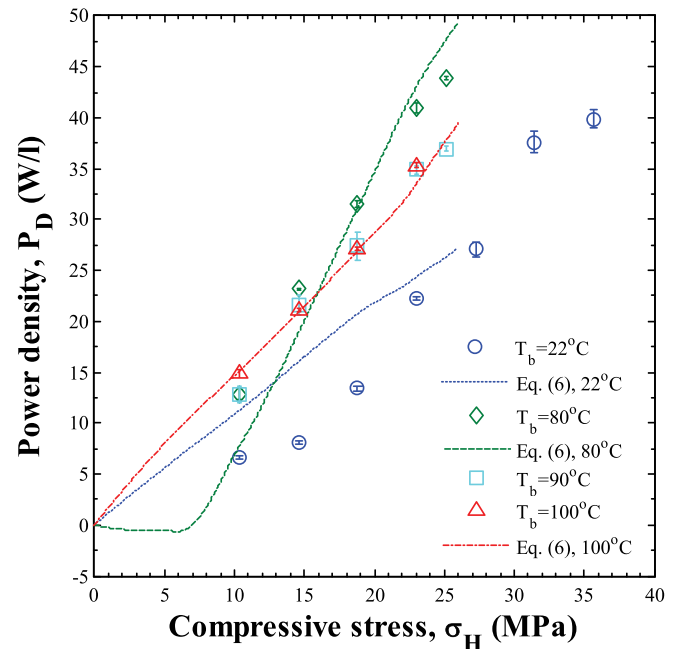

FIG. 6. Experimentally measured power density generated by performing the thermally biased mechanical power cycle on [001] PMN-28PT as a function of compressive stress. The bias-temperature T_b ranged from 22 to $100\,°C$. The frequency was fixed at 1 Hz. The low and high electric fields E_L and E_H were set at 0.2 and 0.8 MV/m. The lines represent the predictions of the model given by Eq. (6) using properties retrieved from bipolar *D-E* loops.

100 °C, the material remained in the highly polarized tetragonal phase away from any phase boundaries for all electric fields considered under zero stress.[13] At these temperatures, the application of large compressive stress during process 2–3 also caused a phase transition into the monoclinic phase. However, the decrease in electric field during process 3–4 did not lead to a phase transition into the orthorhombic phase. This interpretation is supported by extrapolation of the [001] PMN-32PT phase diagram reported in Ref. 15 to PMN-28PT at 90 °C and 100 °C. This resulted in nearly identical power density generated versus compressive stress at these temperatures.

Furthermore, for cycles performed at 22 °C, the material transitioned from the rhombohedral to the monoclinic phase during process 1–2, as suggested by the PMN-28PT phase diagram at zero stress.[13] Then, for large compressive stress σ_H, the sample transitioned into the orthorhombic phase during process 3–4, as suggested by the PMN-32PT phase diagram.[15] Overall, the power density with $T_b = 22$ °C was limited by the fact that the sample never reached the highly polarized tetragonal phase. These results indicate that to maximize power generation of PMN-28PT, the new cycle should be performed at temperatures where the tetragonal phase is present. In addition, the compressive stress σ_H should be large enough to induce the orthorhombic phase at the temperature and electric field corresponding to state 2 of the cycle.

3. Effect of frequency

Figure 7 shows the power density generated by the thermally biased mechanical power cycle as a function of compressive stress σ_H for frequency of 0.5, 1, 2, and 3 Hz. The
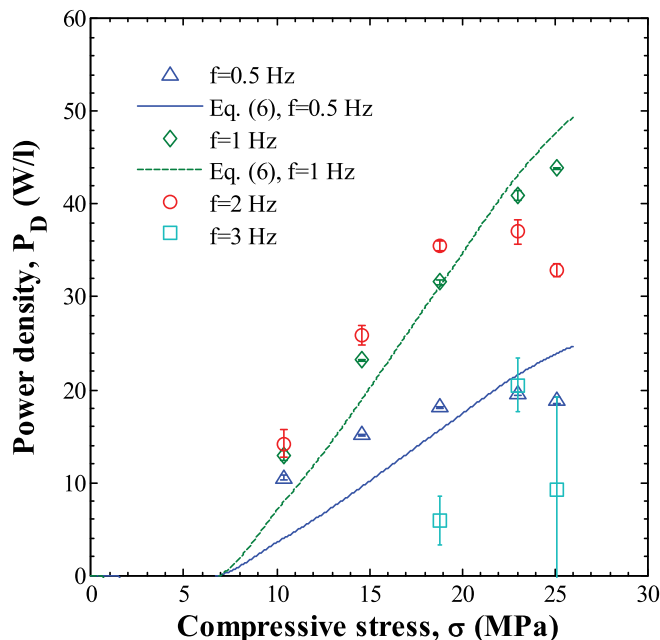

FIG. 7. Experimentally measured power density generated by performing the new power cycle on [001] PMN-28PT as a function of compressive stress σ_H for frequency ranging from 0.5 to 3 Hz. The bias-temperature T_b was maintained at 80 °C. The low and high electric fields E_L and E_H were set at 0.2 and 0.8 MV/m. The lines represent the predictions of the model given by Eq. (6) using properties retrieved from bipolar *D-E* loops.

low and high electric fields E_L and E_H were set at 0.2 and 0.8 MV/m, and the bias-temperature T_b was 80 °C. Each data point represents an average over five cycles and the error bars correspond to one standard deviation or 63% confidence interval. It is evident that the power density increased with increasing compressive stress for frequency below 1 Hz. However, at higher frequency, the power density reached a maximum at compressive stress of 23.02 MPa and decreased beyond. This can be attributed to the fact that, at high cycle frequency, the electric displacement did not reach its equilibrium value during processes 2–3 and 4-1. Furthermore, the large error bars for frequency of 3 Hz were due to inconsistent changes in electric displacement during each process from one cycle to the next. Figure 7 establishes that a cycle frequency of 1 Hz yields the largest power density for large compressive stress at 80 °C.

C. Model predictions

Figure 6 compares experimental data and model predictions obtained from Eq. (6) for the power density P_D at bias-temperature T_b of 22, 80, and 100 °C. Predictions were based on the dielectric properties previously estimated from isothermal bipolar *D-E* loops measured at these temperatures. Analysis of the electric displacement variations $D(t)$-D_4 versus time t with $T_b = 80$ °C for cycle frequency ranging from 0.5 to 2 Hz confirmed that the properties extracted from the *D-E* loops at 0.1 Hz can be used in the model given by Eq. (6) (see supplementary material[33]). However, predictions for $T_b = 90$ °C were not included because isothermal *D-E* loops were not collected at 90 °C. Figure 6 indicates that the model predictions agreed well with experimental data. In fact, the average relative error between experimental data and model predictions was 47.6%, 13.9%, and 2.4% for T_b equal to 22, 80, and 100 °C, respectively. The largest error for $T_b = 22$ °C corresponded to small values of σ_H. Overall, the model predictions were acceptable.

Figure 7 shows the model predictions of the power density at $T_b = 80$ °C for frequency of 0.5 and 1 Hz. Here also, the model yields reasonable predictions. In fact, the average relative error between experimental data and model predictions at 0.5 and 1 Hz was 29.1% and 13.9%, respectively. Note that the model did not yield accurate predictions for frequencies larger than 1 Hz because then, the cycle did not follow the path of the *D-E* loops at 0.1 Hz. In other words, D did not reach its equilibrium value during processes 2–3 and 4-1 as previously discussed. Overall, these results validate the model for P_D given by Eq. (6). It can be used to predict energy ($N_D = P_D/f$) and power densities from the material dielectric properties.

D. Material efficiency

Figure 8(a) presents the relative electric displacement D-D_4 as a function of electric field E experimentally measured during the new thermally biased mechanical cycle performed at $T_b = 80$ °C and $T_b = 100$ °C at low frequency $f \sim 0.004$ Hz with $E_L = 0.2$ MV/m, $E_H = 0.8$ MV/m, and $\sigma_H = 25$ MPa. Figure 8(b) shows the corresponding experimentally measured stress σ versus relative strain x-x_1. The

(a)

(b)
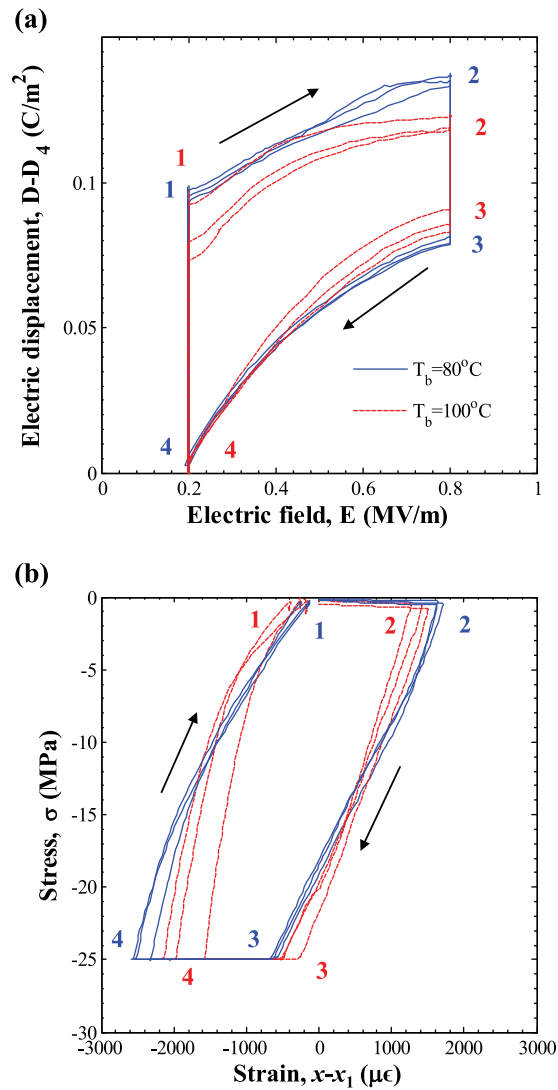
FIG. 8. (a) Experimentally measured stress versus strain diagrams for the thermally biased mechanical power cycle performed at $T_b = 80\,°C$ and $100\,°C$. (b) Experimentally measured electric displacement versus electric field diagrams for the thermally biased mechanical power cycle performed $T_b = 80\,°C$ and $100\,°C$. In all cases $E_L = 0.2\,MV/m$, $E_H = 0.8\,MV/m$, and $\sigma_H = 25\,MPa$.

energy density N_D was measured as 39.7 ± 1.0 and $31.2 \pm 1.0\,J/l/cycle$ and the mechanical work W_{in} was 53.1 ± 1.3 and $47.7 \pm 3.1\,J/l/cycle$ for cycles performed at 80 and $100\,°C$, respectively. The corresponding material efficiency η, given by Eq. (2), was equal to $74.6\% \pm 0.1\%$ and $65.3\% \pm 3.3\%$, respectively. Note that the heat input Q_{in} was taken as zero, thanks to the bias-temperature kept constant during the cycle. These large efficiencies demonstrate that the material undergoing the new cycle was very efficient at converting mechanical energy into electrical energy. The largest energy density, power density, and material efficiency were obtained at $80\,°C$, thanks to the tetragonal-monoclinic-orthorhombic phase transition sequence resulting in large changes in electric displacement, as previously discussed. In addition, less mechanical energy was required to cause these phase transitions at $80\,°C$ than at 90 or $100\,°C$. At $100\,°C$, the PMN-28PT sample had not transitioned to the orthorhombic phase for the stresses considered. This is

illustrated in Figure 8 by the fact that increasing compressive stress from 0 to 25 MPa during process 2–3 produced a larger change in (i) strain and (ii) electric displacement at $80\,°C$ than at $100\,°C$.

Finally, the maximum material efficiency of $87.3\% \pm 5.6\%$ was obtained at low frequency $f \sim 0.004\,Hz$ with $T_b = 85\,°C$, $E_L = 0.2\,MV/m$, $E_H = 0.95\,MV/m$, and $\sigma_H = 34\,MPa$. Under these conditions, $N_D = 47.8 \pm 1.4\,J/l/cycle$ and $W_{in} = 54.9 \pm 1.9\,J/l/cycle$. These operating conditions were the same as those that yielded the maximum material efficiency of 64.1% for our thermomechanical power cycle.[21] Thus, the thermally biased mechanical power cycle achieved larger material efficiency by replacing the thermal cycling in the thermomechanical power cycle with a temperature-bias.

E. Comparison with other direct mechanical energy conversion methods

Table I compares the operating frequency as well as the power and energy densities experimentally harvested using various direct mechanical energy conversion methods. Roundy *et al.*[19] used a piezoelectric lead zirconate titantate (PZT) linear bimorph cantilever driven at a resonant frequency of 120 Hz and acceleration of $2.5\,m/s^2$ to harvest $0.98\,W/l$. However, the large beam deflections required to induce large strains in the PZT were only achievable at frequency near the resonance frequency. Alternatively, Wang and Yuan[31] applied a time-varying magnetic field to PZT sandwiched between magnetostrictive Terfenol-D layers to harvest $0.9\,W/l$ at 58 Hz. The outer Terfenol-D layers were able to induce larger strains in the piezoelectric PZT than the traditional bending approach.[31] This resulted in larger energy density than the linear piezo bimorph method. However, the smaller cycle frequency caused the two methods to achieve similar power densities. In addition, Cottinet *et al.*[32] applied cyclic transverse strain of 0.2% at 100 Hz to electrostrictive terpolymer poly(vinylidene fluoride-trifluoroethylene-chlorofluoroethylene) [P(VDF-TrFE-CFE)] films containing 1 vol. % carbon black and harvested $0.015\,W/l$. In this case, a bias electric field of $5\,MV/m$ was applied continuously throughout the cycle.[32] Moreover, Dong *et al.*[20] applied cyclic compressive stress between 20 and 26 MPa at 1 Hz in the [001] direction to [110]-poled piezoelectric PIN-PMN-PT single crystals at room temperature. The increase in compressive stress induced a phase transition that increased the polarization of the material and its subsequent decrease induced the reverse phase transition. The resulting power density

TABLE I. Comparison of frequency, maximum power density, and energy density experimentally measured using different methods of mechanical to electrical energy conversion.

Conversion method	f (Hz)	Max P_D (W/l)	N_D (J/l/cycle)	Ref.
Linear piezo bimorph	120	0.98	0.008	19
Magnetostrictive	58	0.9	0.0015	31
Electrostrictive polymer	100	0.015	0.0002	32
Mechanical phase change	1	0.75	0.75	20
Thermally biased mechanical cycle	1	44	44	Present

harvested from this cycle was 0.75 W/l corresponding to the largest energy density $N_D = 0.75$ J/l/cycle among the previously mentioned mechanical energy harvesting methods.[20] Note that this solid-state phase change method did not have performance peaks limited to resonant frequency.[20] In addition, it differed from the new cycle in that (i) it was performed in the absence of an applied electric field and (ii) compressive stress was used to increase rather than decrease the polarization of the material. Table I indicates that the present thermally biased mechanical cycle generated energy and power densities orders of magnitude larger than other popular methods using piezoelectric materials. However, in the present study, the energy generated was not harvested, unlike the other conversion methods. Thus, it is critical to design an electric circuit to condition the power and to harvest the energy generated by the new cycle.

V. CONCLUSION

This study demonstrated a novel thermally biased mechanical power cycle on ferroelectric [001]-poled PMN-28PT single crystals. Maximum energy and power densities of 44 J/l/cycle and 44 W/l were achieved at 1 Hz for bias-temperature T_b of 80 °C and electric field cycled between 0.2 and 0.8 MV/m with compressive stress $\sigma_H = 25.13$ MPa. In addition, the power density increased with increasing compressive stress for cycle frequency less than or equal to 1 Hz. For higher cycle frequency, the power density reached a maximum for compressive stress equal to $\sigma_H = 23.03$ MPa. The maximum power density of the new cycle was obtained for temperature bias of 80 °C, thanks to tetragonal to monoclinic to orthorhombic phase transition sequence during the cycle resulting in large changes in electric displacement. The material efficiency of this new power cycle exceeded that of the thermomechanical power cycle previously presented.[21] The energy and power densities generated by the new cycle were orders of magnitude larger than alternative mechanical energy conversion methods. Finally, a physics-based model predicting the power density was derived and validated against experimental data. It can be used to predict the energy and power densities for any material based on their dielectric properties and the operating electric fields, temperature, and frequency.

ACKNOWLEDGMENTS

[1]Lawrence Livermore National Laboratory and Department of Energy, U.S. Energy Flow Trends - 2012, May 2013.

[2]D. G. Thombare and S. K. Verma, "Technological development in the Stirling cycle engines," Renewable Sustainable Energy Rev. **12**, 1–38 (2008).

[3]H. Chen, D. Y. Goswami, and E. K. Stefanakos, "A review of thermodynamic cycles and working fluids for the conversion of low-grade heat," Renewable Sustainable Energy Rev. **14**, 3059–3067 (2010).

[4]S. B. Riffat and X. Ma, "Thermoelectrics: A review of present and potential applications," Appl. Therm. Eng. **23**, 913–935 (2003).

[5]M. Zebarjadi, K. Esfarjani, M. S. Dresselhaus, Z. F. Ren, and G. Chen, "Perspectives on thermoelectrics: From fundamentals to device applications," Energy Environ. Sci. **5**, 5147–5162 (2012).

[6]G. Despesse, J. J. Chaillout, S. Boisseau, and C. Jean-Mistral, "Mechanical energy harvesting," *Energy Autonomous Micro and Nano Systems* (John Wiley & Sons, Inc., Hoboken, NJ, 2012).

[7]M. E. Lines and A. M. Glass, *Principles and Applications of Ferroelectrics and Related Materials* (Clarendon Press, Oxford, UK, 1977).

[8]S. B. Lang and D. K. Das-Gupta, *Handbook of Advanced Electronic and Photonic Materials and Devices* (Academic Press, San Diego, CA, 2001), Vol. 4.

[9]Z. Li, Z. Xi, Z. Xu, and X. Yao, "Dielectric/ferroelectric response and phase transition of PMN-0.32PT single crystal," J. Mater. Sci. Lett. **21**, 1325–1327 (2002).

[10]S. E. Park and T. R. Shrout, "Ultrahigh strain and piezoelectric behavior in relaxor based ferroelectric single crystals," J. Appl. Phys. **82**(4), 1804 (1997).

[11]Z.-G. Ye and M. Dong, "Morphotropic domain structures and phase transitions in relaxor-based piezo-/ferroelectric (1-x)PbMg$_{1/3}$Nb$_{2/3}$O$_3$-xPbTiO$_3$ single crystals," J. Appl. Phys. **87**(5), 2312 (2000).

[12]D. Zhou, F. Wang, L. Luo, J. Chen, W. Ge, X. Zhao, and H. Luo, "Characterization of complete electromechanical constants of rhombohedral 0.72Pb(Mg$_{1/3}$Nb$_{2/3}$)-0.28PbTiO$_3$ single crystals," J. Phys. D **41**, 185402 (2008).

[13]A. Herklotz, J. D. Plumhof, A. Rastelli, O. G. Schmidt, L. Schultz, and K. Dorr, "Electrical characterization of PMN-28%PT(001) crystals used as thin-film substrates," J. Appl. Phys. **108**, 094101 (2010).

[14]Y. Guo, H. Luo, D. Ling, H. Xu, T. He, and Z. Yin, "The phase transition sequence and the location of the morphotropic phase boundary region in (1-x)Pb(Mg$_{1/3}$Nb$_{2/3}$)O$_3$-xPbTiO$_3$ single crystal," J. Phys.: Condens. Matter **15**(2), L77–L82 (2003).

[15]E. A. McLaughlin, T. Liu, and C. S. Lynch, "Relaxor ferroelectric PMN-32PT crystals under stress, electric field and temperature loading: II-33-mode measurements," Acta Mater. **53**(14), 4001–4008 (2005).

[16]Q. Wan, C. Chen, and Y. P. Shen, "Effects of stress and electric field on the electromechanical properties of Pb(Mg$_{1/3}$Nb$_{2/3}$)O$_3$-0.32PbTiO$_3$ single crystals," J. Appl. Phys. **98**, 024103 (2005).

[17]J. Chen, H. Fan, S. Ke, X. Chen, C. Yang, and P. Fang, "Relaxor behavior and dielectric properties of lead magnesium niobate-lead titanate thick films prepared by electrophoresis deposition," J. Alloys Compd. **478**, 853–857 (2009).

[18]R. B. Olsen, D. A. Bruno, J. M. Briscoe, and W. F. Butler, "A pyroelectric energy converter which employs regeneration," Ferroelectrics **38**, 975–978 (1981).

[19]S. Roundy and P. K. Wright, *Energy Scavenging for Wireless Sensor Networks: With Special Focus on Vibrations* (Kluwer Academic Publishers, Boston, MA, 2004).

[20]W. Dong, P. Finkel, A. Amin, and C. S. Lynch, "Mechanical energy harvesting utilizing phase transition in 32 mode relaxor-ferroelectric PIN-PMN-PT single crystals," *SPIE Smart Structures and Materials+ Nondestructive Evaluation and Health Monitoring* (International Society for Optics and Photonics, 2012), 834308.

[21]I. M. McKinley, F. Y. Lee, and L. Pilon, "A novel thermoelectromechanical energy conversion cycle," Appl. Energy (unpublished).

[22]C. S. Lynch, "The effect of uniaxial stress on the electro-mechanical response of 8/65/35 PLZT," Acta Mater. **44**, 4137–4139 (1996).

[23]Z. Feng, D. Lin, H. Luo, S. Li, and D. Fang, "Effect of uniaxial stress on the electromechanical response of ⟨001⟩-oriented Pb(Mg$_{1/3}$Nb$_{2/3}$)O$_3$-PbTiO$_3$ crystals," J. Appl. Phys. **97**, 024103 (2005).

[24]F. P. Beer, Jr., E. R. Johnston, and J. T. DeWolf, *Mechanics of Materials*, 4th ed. (McGraw-Hill, New York, NY, 2006).

[25]R. Kandilian, A. Navid, and L. Pilon, "Pyroelectric energy harvesting capabilities of PMN-PT near the morphotropic phase boundary," Smart Mater. Struct. **20**(5), 055020 (2011).

[26]A. Navid and L. Pilon, "Pyroelectric energy harvesting using Olsen cycle in purified and porous poly(vinylidene fluoride-trifluoroethylene) [P(VDF-TrFE)] thin films," Smart Mater. Struct. **20**, 025012 (2011).

[27]I. M. McKinley, R. Kandilian, and L. Pilon, "Waste heat energy harvesting using the Olsen cycle on 0.945Pb(Zn$_{1/3}$Nb$_{2/3}$)O$_3$-0.055PbTiO$_3$ single crystals," Smart Mater. Struct. **21**(3), 035015 (2012).

[28]F. Y. Lee, S. Goljahi, I. M. McKinley, C. S. Lynch, and L. Pilon, "Pyroelectric waste heat energy harvesting using relaxor ferroelectric

8/65/35 PLZT and the Olsen cycle," Smart Mater. Struct. **21**, 025021 (2012).

[29]T. Chin, F. Y. Lee, I. M. McKinley, S. Goljahi, C. S. Lynch, and L. Pilon, "Pyroelectric waste heat energy harvesting using 9.5/65/35 PLZT ceramics," IEEE Trans. Ultrason., Ferroelectr., Freq. Control **59**, 2373 (2012).

[30]I. M. McKinley and L. Pilon, "Phase transitions and thermal expansion in pyroelectric energy conversion," Appl. Phys. Lett. **102**, 023906 (2013).

[31]L. Wang and F. G. Yuan, "Vibration energy harvesting by magnetostrictive material," Smart Mater. Struct. **17**, 045009 (2008).

[32]P. J. Cottinet, D. Guyomar, M. Lallart, B. Guiffard, and L. Lebrun, "Investigation of electrostrictive polymer efficiency for mechanical energy harvesting," IEEE Trans. Ultrason., Ferroelectr., Freq. Control **58**, 1842 (2011).

[33]See supplementary material at http://dx.doi.org/10.1063/1.4846735 for additional discussion on the effect of frequency.